

A model-based investigation of the recent rebound of shelf water salinity in the Ross Sea

Jingwei ZHANG¹, Xuebin Zhang², Matt A King¹, and Kewei Lyu³

¹University of Tasmania

²Commonwealth Scientific and Industrial Research Organisation (CSIRO)

³Xiamen University

August 12, 2024

Abstract

Intense atmosphere-ocean-ice interactions in the Ross Sea play a vital role in global overturning circulation by supplying saline and dense shelf waters. Since the 1960s, freshening of the Ross Sea shelf water has led to a decline in Antarctic Bottom Water formation. Since the early 2010s, however, the salinity of the western Ross Sea has rebounded. This study adopts an ocean-sea ice model to investigate the causes of this salinity rebound. Model-based salinity budget analysis indicates that the salinity rebound was driven by increased brine rejection from sea ice formation, triggered by the nearly equal effects of local anomalous winds and surface heat flux. The local divergent wind anomalies promoted local sea ice formation by creating a thin ice area, while a cooling heat flux anomaly decreased the surface temperature, increasing sea ice production. This highlights the importance of understanding local climate variability in projecting future dense shelf water change.

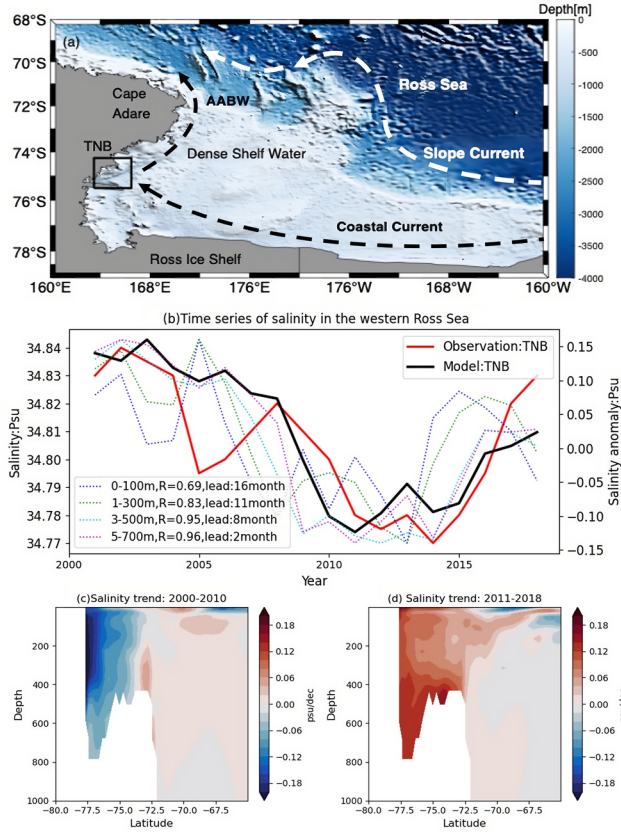


Figure 1: This is a caption

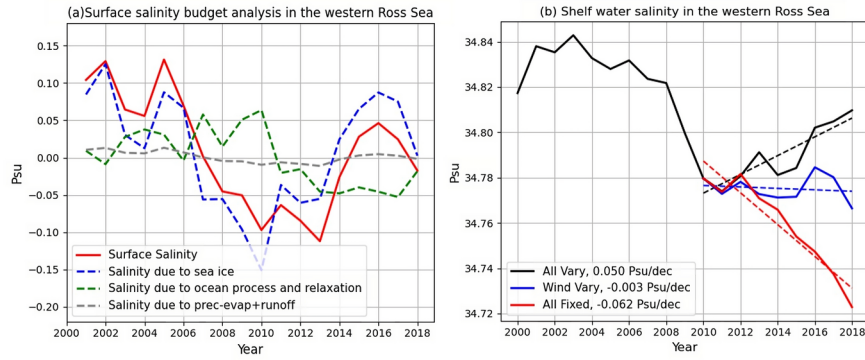


Figure 2: This is a caption

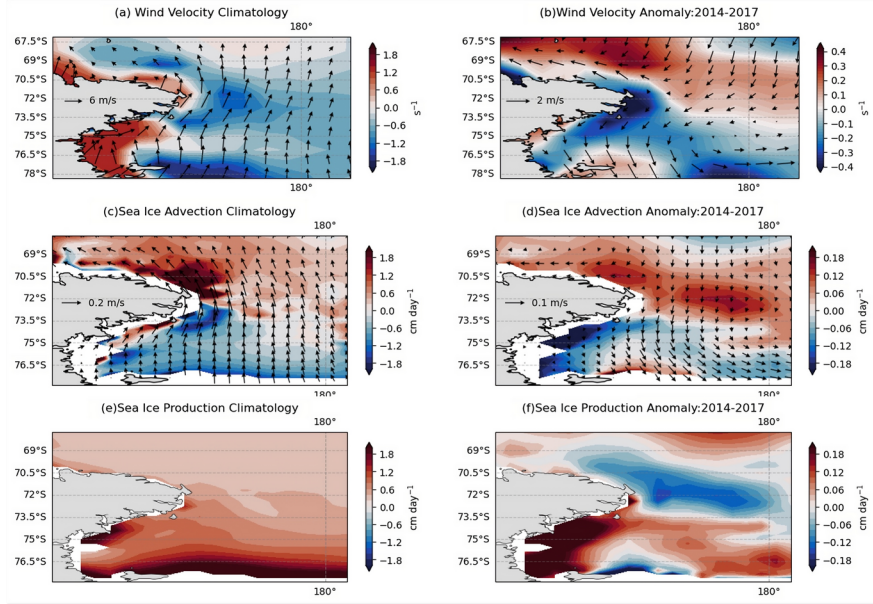


Figure 3: This is a caption

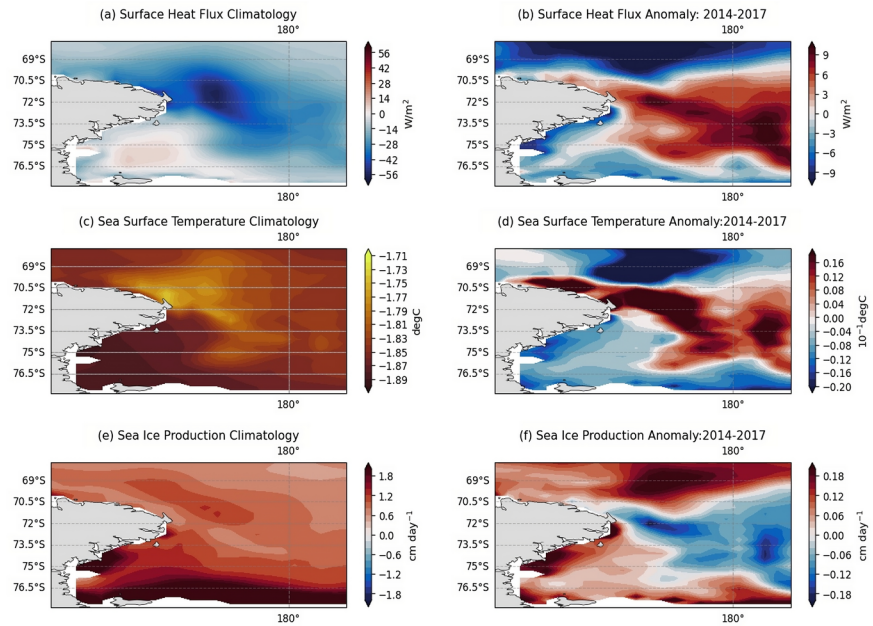


Figure 4: This is a caption



Geophysical Research Letters

Supporting Information for

A model-based investigation of the recent rebound of shelf water salinity in the Ross Sea

Jingwei Zhang^{1,2}, Xuebin Zhang², Matt A. King^{1,3}, Kewei Lyu⁴

¹School of Geography, Planning, and Spatial Sciences, University of Tasmania, Hobart, Australia

²Climate Science Centre, CSIRO Environment, Hobart, Australia

³The Australian Centre for Excellence in Antarctic Science, University of Tasmania, Hobart, Australia

⁴State Key Laboratory of Marine Environmental Science, Center for Marine Meteorology and Climate Change, College of Ocean and Earth Sciences, Xiamen University, Xiamen, China

Overview

We present here additional information related to oceanography data, model simulation setup, summary of perturbation experiment settings, and the additional experiment and analysis.

Contents of this file

1. Text 1.1-1.5
2. Table S1
3. Figures S1-S10

Corresponding authors:

Jingwei Zhang (jingwei.zhang@utas.edu.au)

Xuebin Zhang (xuebin.zhang@csiro.au)

Text

1.1 Oceanography data

The oceanographic data utilized in this study were sourced from the work of Castagno et al. (2019). To capture the salinity changes in the Deep Shelf Water (DSW) of the Ross Sea, specific regions were selected for analysis. The time series in **Figures 1b and S1** were obtained by averaging the salinity in the 30 dbar layer from 870 to 900 dbar for TNB (74.25°S–75.50°S and 163.00°E–166.00°E), and in the bottom 20 dbar for Drygalski Trough mouth (DT, 72.00°S and 72.67°S and 171.50°E and 174.50°E), Joides Trough (JT, 73.90°S–74.10°S and 174.20°E–176.00°E) and Glomar Challenger Trough (GCT, 75.80°S–76.20°S and 178.00°W–177.10°W).

1.2 Climate indices

The Southern Oscillation Index (SOI) captures climate variability associated with the El Niño/La Niña cycle and represents the dominant modes of climate variability in the Pacific sector of the Southern Ocean. We used monthly SOI provided by NCAR (<https://climatedataguide.ucar.edu/climate-data/southern-oscillation-indices-signal-noise-and-tahitidarwin-slp-soi>). The monthly location of ASL central was also used in this study, sourced from (https://scotthosking.com/asl_index). The location of ASL central, which is the minimum sea surface pressure, is defined using an ASL detection methodology, described in (Hosking et al., 2016).

1.3 Sea ice production in the Ross Sea polynya

Large uncertainties exist in estimating sea ice production across the entire Ross Sea continental shelf, primarily due to a scarcity of in-situ observations during the autumn-winter period (Ackley et al., 2020). We thus compared our model results with the recent reconstructed sea ice production in the Ross Sea polynyas, which are relatively better

observed than other regions. This reconstructed data, sourced from the work of Nihashi et al. (2023), provided a time series of ice production in the Ross Sea polynyas from 2002 (**Figure S10**), derived using high spatial resolution satellite data from passive microwave sensors, including the Advanced Microwave Scanning Radiometer for EOS and the Advanced Microwave Scanning Radiometer 2. Ice production estimates in the Ross Sea polynya were derived from heat flux calculations for the March–October period following the previous studies (Nihashi & Ohshima, 2015; Nihashi et al., 2017; Tamura et al., 2008). And the polynya was defined as an area comprising sea-ice pixels with a SIC of $\geq 30\%$ and a thickness of ≤ 20 cm.

1.4 Model simulation setup

ACCESS-OM2 is a global model with coupled ocean and sea-ice components driven by prescribed atmosphere forcing. The ocean component is the Modular Ocean Model version 5.1 (MOM5.1; (Griffies, 2012) from the National Oceanic and Atmospheric Administration Geophysical Fluid Dynamics Laboratory (NOAA-GFDL). The sea-ice component is the Community Ice Code version 5.1.2 (CICE5.1.2;(Hunke et al., 2015)). The coupling of these two components is achieved by the model coupling toolkit from CERFACS and CNRA through the Ocean Atmospheric Sea Ice Soil version 3 (OASIS3; (Valcke, 2006)). ACCESS-OM2 is initialized from a state of rest, with temperature and salinity fields coming from the World Ocean Atlas 2013 v2 monthly climatology (WOA13) (Locarnini et al., 2013; Zweng et al., 2013). The atmospheric forcing derived from JRA55-do (Tsujino et al., 2018), including wind speed, air temperature and humidity, radiation, precipitation, and sea level pressure, are used to diagnose air–sea fluxes (wind stress, heat flux, and freshwater flux) through bulk formulae and interactive coupling between ocean and sea ice. Freshwater flux and heat flux are defined as positive downward (i.e., freshwater/heat gain by the ocean). The Antarctic

calving and ice shelf basal melting are prescribed as a climatological runoff (Depoorter et al., 2013) near the Antarctic “coast”. We should note that this “idealised” freshwater forcing assumption might be suitable for basal melting that delivers freshwater along with a line source close to the Antarctic coast but may not appropriately represent the non-uniform drifting distribution of freshwater released by iceberg.

In ACCESS-OM2, there are no explicit tides, but the model does include mixing and viscosity from parameterized internal and barotropic tidal processes. During the spin-up, surface salinity was restored to the WOA13 monthly climatology with a restoring time scale of 21 days over the top layer. This model does not include the ice shelf component, and the meltwater from Greenland and Antarctica is replaced by a climatological runoff (Bamber et al., 2012; Depoorter et al., 2013; Kiss et al., 2020).

Meanwhile, despite being a common technique to prevent multi-decadal drift in ocean surface simulation (Griffies et al., 2009), surface relaxations to climatology would limit ocean responses to the applied perturbation. To overcome this limitation, the restoring salt fluxes were saved at 3 hourly intervals over the last 10 years of the spin-up. A new control run was then conducted in a non-adaptive way (Lyu et al., 2023; Zhang & McPhaden, 2008; Zika et al., 2018), in which surface restoring fluxes were prescribed from the above-saved ones. By doing so, the model surface conditions are allowed to respond freely to the applied surface flux perturbation.

The initial phase of our study involves a 200-year spin-up, which is driven by the repeat year forcing from 1st May 1990 through 30th April 1991 (RYF-9091, repeat-year forcing 1990-1991). This repeat year forcing is chosen due to its neutral characteristics with respect to major climate variability modes. Following this spin-up, the ACCESS-OM2 model is then forced with interannually varying atmospheric variables based on the Japanese 55-Year

Reanalysis (JRA-55) dataset for driving ocean–sea ice models version 1.4 (Tsujino et al., 2018) from 1990 to 2018.

1.5 Experiment design:

- All-Fixed (09-10) and Wind-Vary (09-10) experiments

Applying a 10-year climatology may overlook events with high-frequency storms, potentially leading to anomalies in heat flux. Therefore, a repeat year forcing using 2009-2010 (1st May 2009 to 30th April 2010) atmospheric condition (RYF-0910), which includes high-frequency events, has been tested. The All-Fixed (09-10) and Wind-Vary (09-10) experiments, except for the wind forcing in wind experiment, apply the repeated 2009-2010 atmospheric conditions from 2010 to 2018 to simulate the ocean response after 2010, if atmospheric conditions remain constant (**Figure S2**).

- Ross Sea-Only wind experiment

To ascertain the specific location of the wind responsible for the changes in sea ice, we conducted another experiment called the Ross Sea-Only wind experiment. For simplicity, we define the local western Ross Sea as a box area, Area 1 (**Figure S5**, 160°E-170°W, 60-80°S), while Area 2 encompasses the entirety of the Southern Hemisphere (south of 0°) excluding Area 1. The Ross Sea-Only simulation employed climatological forcing as in the All-Fixed experiment, except for the Area 1, where real-time wind forcing was implemented (Table S1). We then compared the Wind-Vary and Ross Sea-Only wind experiments versus the All-Fixed experiment to isolate the impact of local wind stress anomaly in the western Ross Sea.

Table S1 | Summary of experiment simulation settings

Experiment	Wind forcing (Area1)	Wind forcing (Area2)	Other atmospheric forcing
All-Vary	Interannual	Interannual	Interannual
Wind-Vary	Interannual	Interannual	Climatology
All-Fixed	Climatology	Climatology	Climatology
All-Fixed (09-10)	RYP-0910	RYP-0910	RYP-0910
Wind-Vary(09-10)	Interannual	Interannual	RYP-0910
Ross Sea-Only	Interannual	Climatology	Climatology

Note that ‘Interannual’ represents real-time atmospheric forcing, ‘Climatology’ represents the averaged atmospheric condition from 2000 to 2010, and ‘RYP-0910’ represents the repeat year forcing from 1st May 2009 to 30th April 2010. Area 1 is defined as a box area (**Figure S5**, 160°E-170°W, 60-80°S), and Area 2 encompasses the entirety of the Southern Hemisphere (south of 0°) excluding Area 1.

Figures

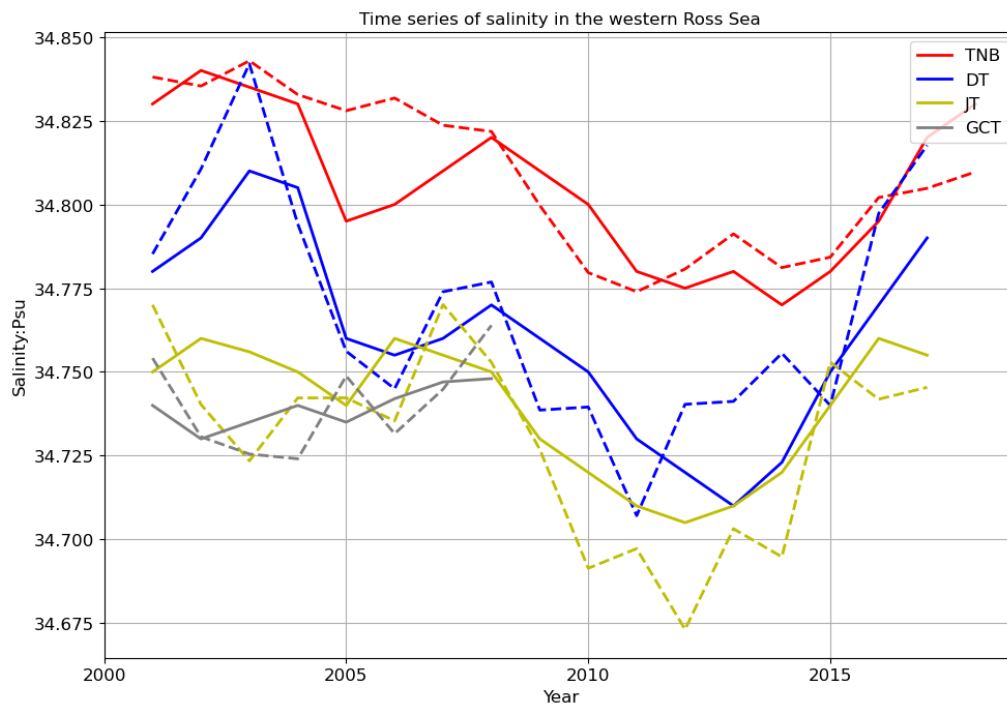


Figure S1 | Comparisons of salinity between model experiments and observations. Time series of averaged DSW salinity measured (solid line) and model-simulated (dashed line) near the seafloor at Terra Nova Bay (TNB, red line), Drygalski Trough mouth (DT, blue line), Joides Trough (JT, yellow line) and Glomar Challenger Trough (GCT, grey line) from 2000 to 2018.

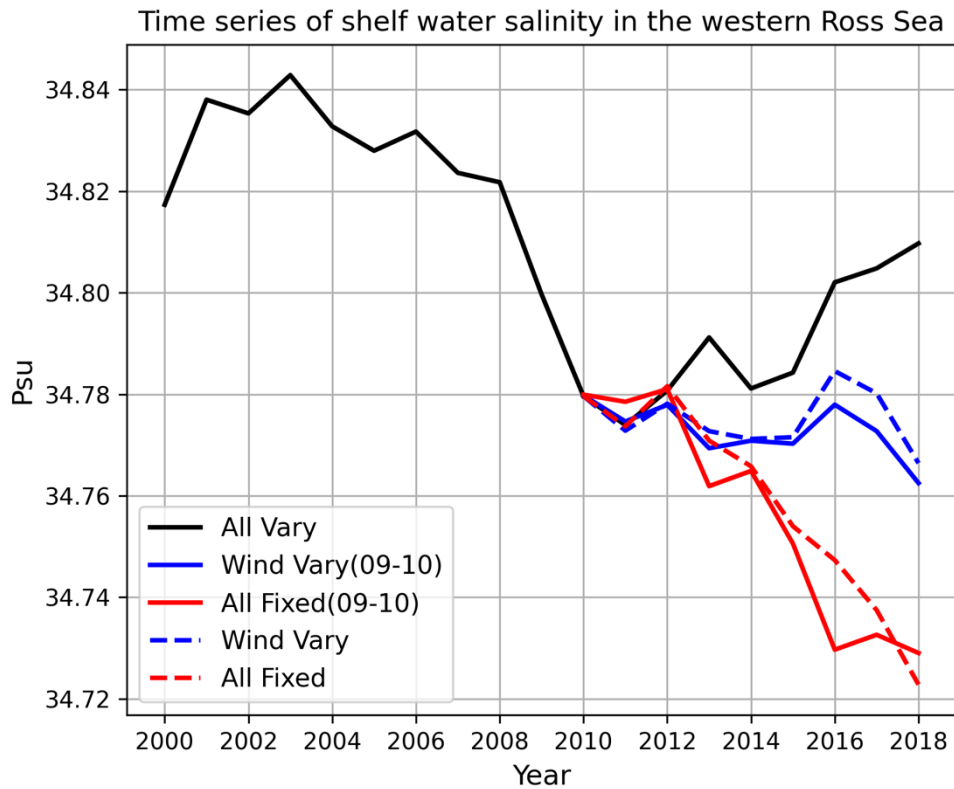


Figure S2 | All-Fixed (09-10) experiment. Same as **Figure 2b**, but instead of being forced by a 10-year climatology, the All-Fixed and Wind-Vary (except wind forcing) models are repeatedly forced by the atmospheric forcing from 2009-2010. The salinity from the Wind-Vary and All-Fixed experiments in Figure 2b are overlaid (dashed red and blue lines).

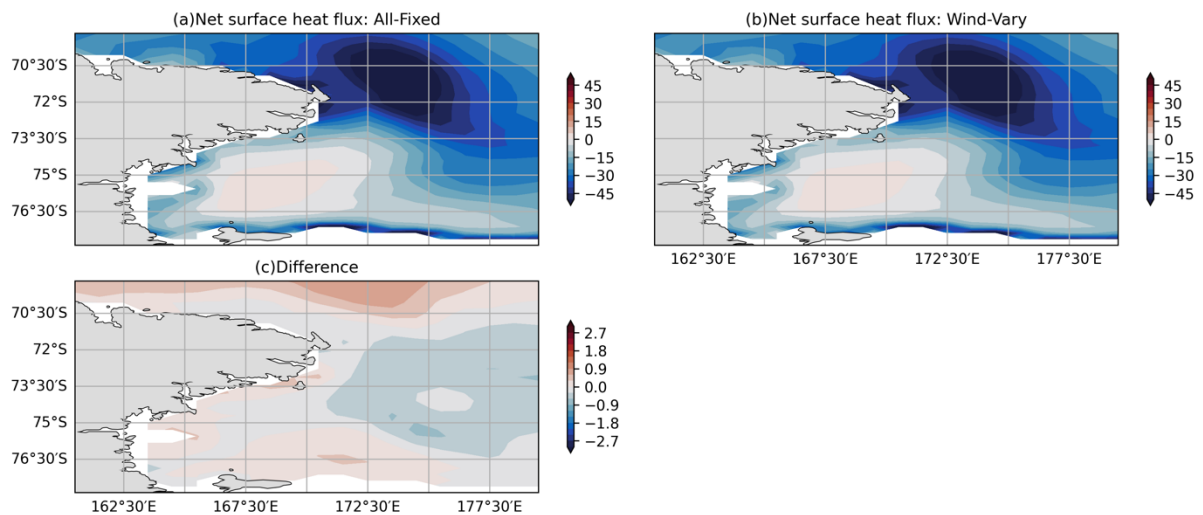


Figure S3 | Net surface heat flux. The averaged net surface heat flux (turbulent flux and radiative flux) from 2014-2017 in All-Fixed experiment (a), Wind-Vary experiment (b), and their difference (c, Wind-Vary minus All-Fixed).

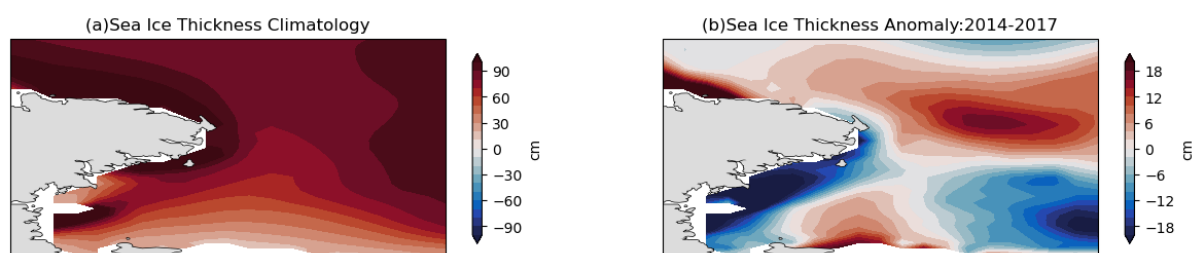


Figure S4 | Sea ice thickness in wind experiment. Climatology (a, All-Fixed) and 2014-2017 anomaly (b, Wind-Vary minus All-Fixed) of sea ice thickness induced by wind forcing.

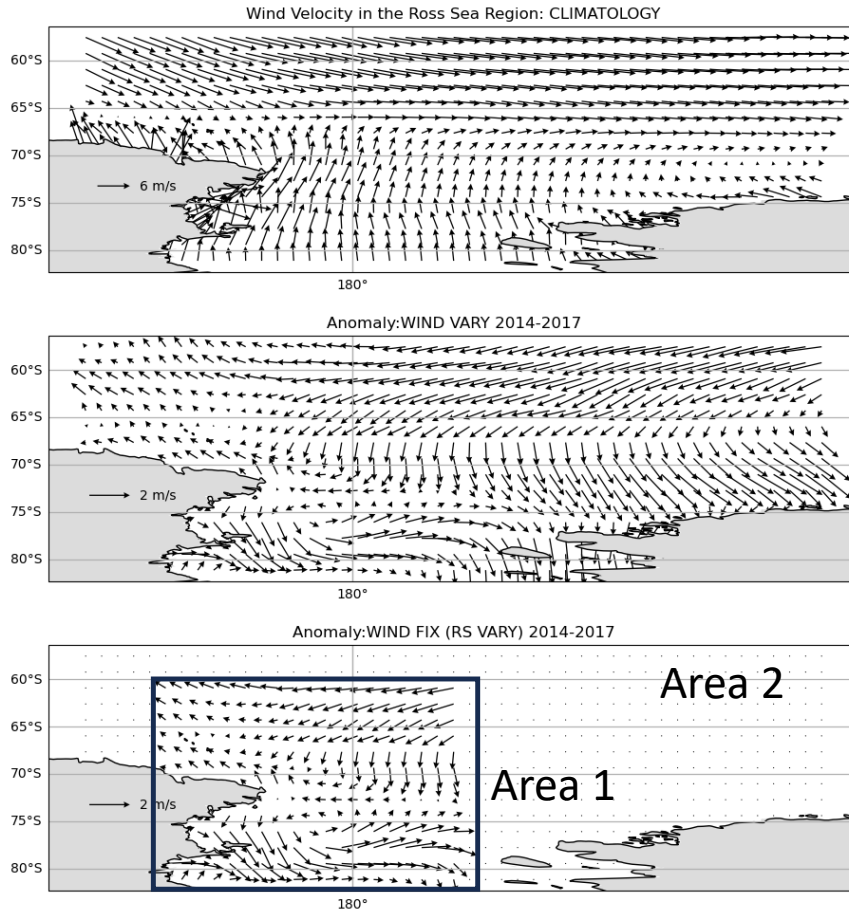


Figure S5 | Interannual variability of winds in the western Ross Sea. The Ross Sea-Only simulation employed climatological forcing as in the All-Fixed experiment for the entire Southern Hemisphere (south of 0°), except for the western Ross Sea (Area 1, 160°E-170°W, 60°S-80°S), where real-time wind forcing was implemented (Table S1).

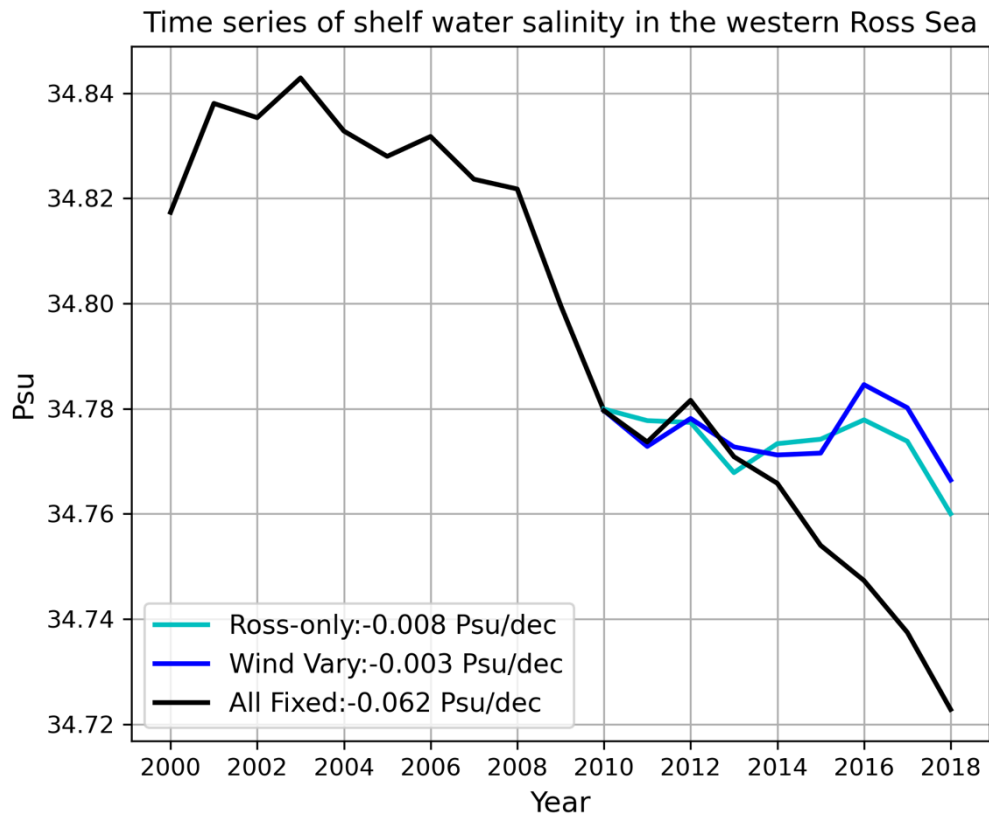


Figure S6 | Simulated DSW salinity from further perturbation experiments. Time series of averaged DSW salinity simulated by All-Fixed experiment (black line) from 2000 to 2018, Wind-Vary (blue line) and Ross Sea-Only (cyan line) from 2010 to 2018 near the seafloor in TNB (details in Supplementary Text 1.4. Ross Sea-Only wind experiment).

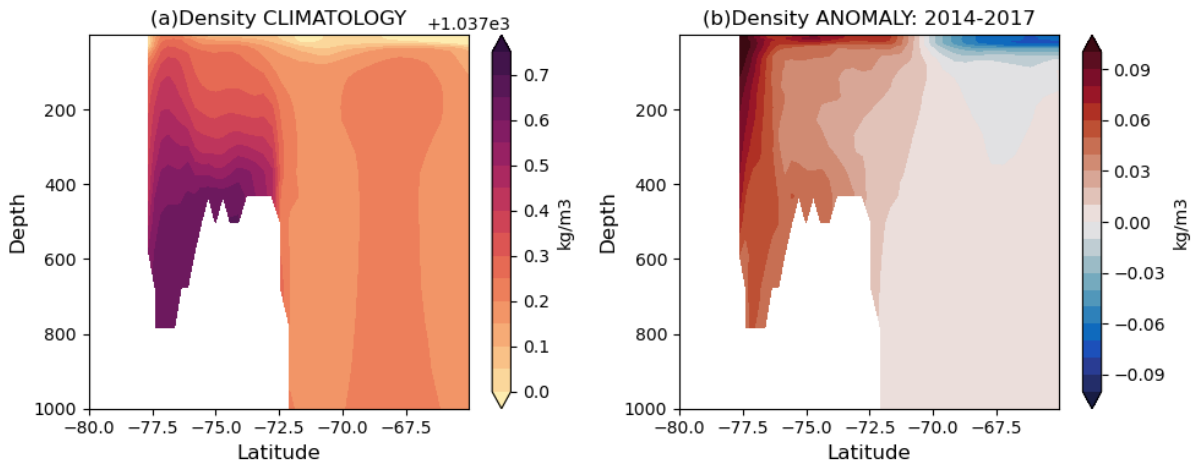


Figure S7 | Density changes in surface heat flux experiment. Zonal averaged (163-170°E) climatology (a, Wind-Vary) and 2014-2017 anomaly (b, All-Vary minus Wind-Vary) of ocean density in heat flux experiment.

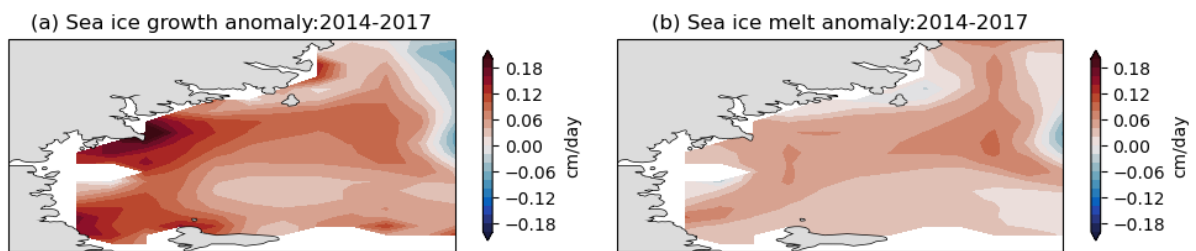


Figure S8 | Sea ice growth and melt in surface heat flux experiment. Averaged sea ice anomalies (All-Vary minus Wind-Vary) in growth (a) and melt (b) between 2014 to 2017 in heat flux experiment.

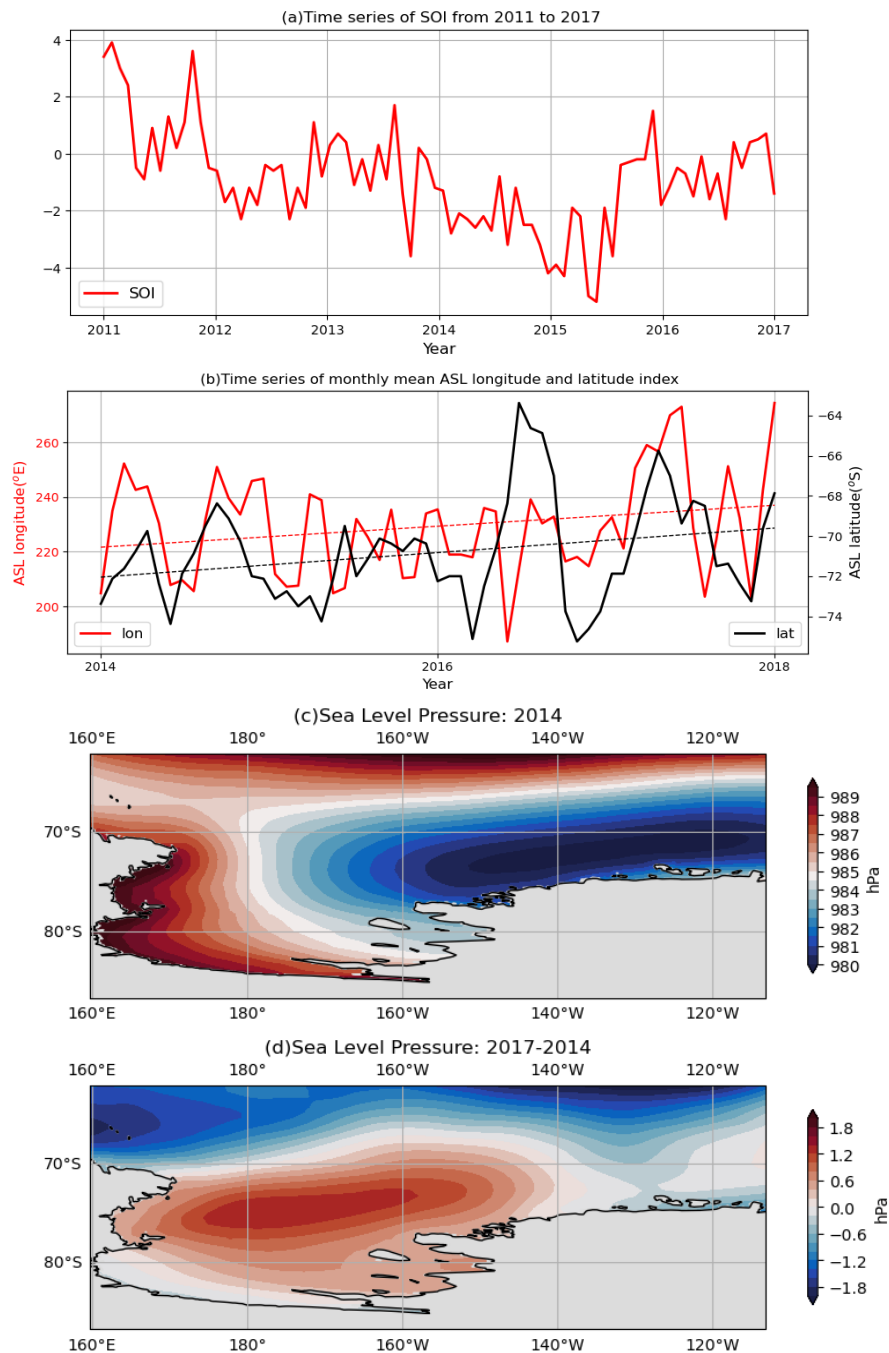


Figure S9 | Wind forcing, and surface heat flux driven by climate anomalies. (a) Time series of SOI between 2011 to 2018. The period from 2014-2017 is characterized by negative SOI. **(b)** Time series (solid line) and trends (dashed line) of ASL central latitude (black line) and longitude (red line) from 2014-2018, within the ASL sector (170°E-298° E, 80°S-60° S). Sea level pressure in 2014 **(c)**, and anomaly in 2017 **(d)**.

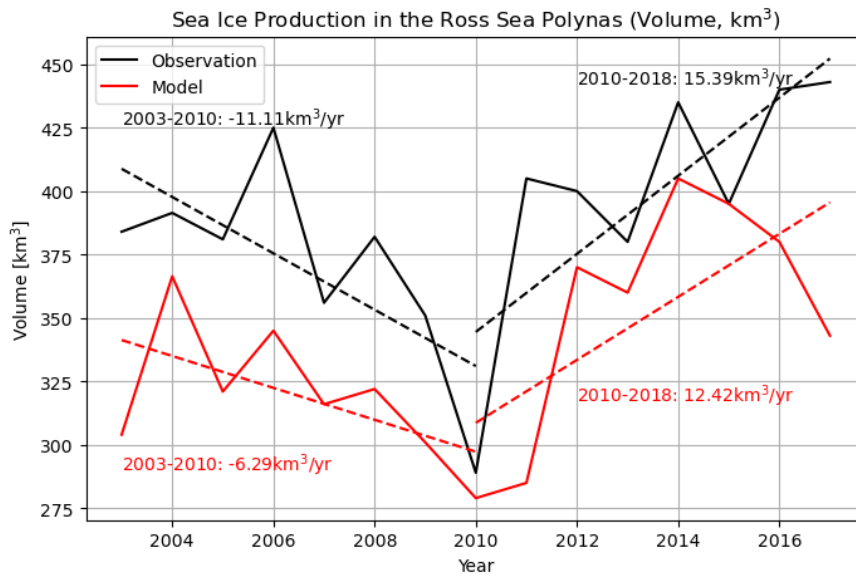


Figure S10 | Sea ice production in the Ross Sea polynya. Time series of observed (solid black line) and simulated (solid red line, All-Vary experiment) annual ice production (cumulative ice production during March–October, volume in km³) and their trends (dashed lines) from 2003-2010 and 2010-2018 in the Ross Sea polynya.

Supplementary References

- Ackley, S., Stammerjohn, S., Maksym, T., Smith, M., Cassano, J., Guest, P., et al. (2020). Sea-ice production and air/ice/ocean/biogeochemistry interactions in the Ross Sea during the PIPERS 2017 autumn field campaign. *Annals of Glaciology*, *61*(82), 181-195.
- Bamber, J., Van Den Broeke, M., Ettema, J., Lenaerts, J., & Rignot, E. (2012). Recent large increases in freshwater fluxes from Greenland into the North Atlantic. *Geophysical research letters*, *39*(19).
- Castagno, P., Capozzi, V., DiTullio, G. R., Falco, P., Fusco, G., Rintoul, S. R., et al. (2019). Rebound of shelf water salinity in the Ross Sea. *Nature Communications*, *10*(1), 1-6.
- Depoorter, M. A., Bamber, J. L., Griggs, J. A., Lenaerts, J. T., Ligtenberg, S. R., van den Broeke, M. R., & Moholdt, G. (2013). Calving fluxes and basal melt rates of Antarctic ice shelves. *Nature*, *502*(7469), 89-92.
- Griffies, S. M. (2012). Elements of the modular ocean model (MOM). *GFDL Ocean Group Tech. Rep*, *7*(620), 47.
- Griffies, S. M., Biastoch, A., Böning, C., Bryan, F., Danabasoglu, G., Chassignet, E. P., et al. (2009). Coordinated ocean-ice reference experiments (COREs). *Ocean Modelling*, *26*(1-2), 1-46.
- Hosking, J. S., Orr, A., Bracegirdle, T. J., & Turner, J. (2016). Future circulation changes off West Antarctica: Sensitivity of the Amundsen Sea Low to projected anthropogenic forcing. *Geophysical research letters*, *43*(1), 367-376.
- Hunke, E., Lipscomb, W., Turner, A., Jeffery, N., & Elliott, S. (2015). CICE: The Los Alamos Sea ice Model Documentation and Software User's Manual Version 5 (Tech. Rep. LA-CC-06-012). *Los Alamos, NM: Los Alamos National Laboratory*.
- Kiss, A. E., Hogg, A. M., Hannah, N., Boeira Dias, F., Brassington, G. B., Chamberlain, M. A., et al. (2020). ACCESS-OM2 v1. 0: a global ocean-sea ice model at three resolutions. *Geoscientific Model Development*, *13*(2), 401-442.
- Locarnini, R., Mishonov, A., Antonov, J., Boyer, T., Garcia, H., Baranova, O., et al. (2013). World Ocean Atlas 2013, Volume 1: Temperature in: NOAA Atlas NESDIS 73 edited by S. In: Levitus.
- Lyu, K., Zhang, X., Church, J. A., Wu, Q., Fiedler, R., & Dias, F. B. (2023). Roles of Surface Forcing in the Southern Ocean Temperature and Salinity Changes under Increasing CO₂: Perspectives from Model Perturbation Experiments and a Theoretical Framework. *Journal of Physical Oceanography*, *53*(1), 19-36.
- Nihashi, S., & Ohshima, K. I. (2015). Circumpolar mapping of Antarctic coastal polynyas and landfast sea ice: Relationship and variability. *Journal of Climate*, *28*(9), 3650-3670.
- Nihashi, S., Ohshima, K. I., & Tamura, T. (2017). Sea-ice production in Antarctic coastal polynyas estimated from AMSR2 data and its validation using AMSR-E and SSM/I-SSMIS data. *IEEE Journal of Selected Topics in Applied Earth Observations and Remote Sensing*, *10*(9), 3912-3922.
- Nihashi, S., Ohshima, K. I., & Tamura, T. (2023). Reconstruct the AMSR-E/2 thin ice thickness algorithm to create a long-term time series of sea-ice production in Antarctic coastal polynyas. *Polar Science*, 100978.
- Tamura, T., Ohshima, K. I., & Nihashi, S. (2008). Mapping of sea ice production for Antarctic coastal polynyas. *Geophysical Research Letters*, *35*(7).

- Tsujino, H., Urakawa, S., Nakano, H., Small, R. J., Kim, W. M., Yeager, S. G., et al. (2018). JRA-55 based surface dataset for driving ocean–sea-ice models (JRA55-do). *Ocean Modelling*, 130, 79-139.
- Valcke, S. (2006). *OASIS User guide, prism 2-5, PRISM-Support Initiative*. Retrieved from
- Zhang, X., & McPhaden, M. J. (2008). Eastern equatorial Pacific forcing of ENSO sea surface temperature anomalies. *Journal of climate*, 21(22), 6070-6079.
- Zika, J. D., Skliris, N., Blaker, A. T., Marsh, R., Nurser, A. G., & Josey, S. A. (2018). Improved estimates of water cycle change from ocean salinity: The key role of ocean warming. *Environmental Research Letters*, 13(7), 074036.
- Zweng, M., Reagan, J., Antonov, J., Locarnini, R., Mishonov, A., Boyer, T., et al. (2013). World Ocean atlas 2013. Vol. 2. Salinity. NOAA Atlas NESDIS 74. In: Silver Spring, MD: National Oceanic and Atmospheric Administration, National

1 **A model-based investigation of the recent rebound of shelf water salinity in**
2 **the Ross Sea**

3 **Jingwei Zhang^{1,2}, Xuebin Zhang², Matt A. King^{1,3} and Kewei Lyu⁴**

4 ¹School of Geography, Planning, and Spatial Sciences, University of Tasmania, Hobart, Australia

5 ²Climate Science Centre, CSIRO Environment, Hobart, Australia

6 ³The Australian Centre for Excellence in Antarctic Science, University of Tasmania, Hobart, Australia

7 ⁴State Key Laboratory of Marine Environmental Science, Center for Marine Meteorology and Climate Change,
8 College of Ocean and Earth Sciences, Xiamen University, Xiamen, China

9

10

11 Corresponding authors:

12 Jingwei Zhang (jingwei.zhang@utas.edu.au)

13 Xuebin Zhang (xuebin.zhang@csiro.au)

14

15

16

17

18

19

20

21

22 **Key Points**

- 23 • Using a global ocean-sea ice model, we simulate the recent rebound of Dense Shelf
24 Water salinity in the western Ross Sea during 2012-2018.
- 25 • A model-based salinity budget analysis reveals increased sea ice formation as the
26 primary driver of the observed salinity rebound.
- 27 • Experiments indicate that this increased sea ice formation is triggered by the
28 combined effect of local wind stress and surface heat flux.

29 **Abstract**

30 Intense atmosphere-ocean-ice interactions in the Ross Sea play a vital role in global
31 overturning circulation by supplying saline and dense shelf waters. Since the 1960s,
32 freshening of the Ross Sea shelf water has led to a decline in Antarctic Bottom Water
33 formation. However, during 2012-2018, salinity of the western Ross Sea has rebounded. This
34 study adopts a global ocean-sea ice model to investigate the causes of this salinity rebound.
35 Model-based surface salinity budget analysis indicates that the salinity rebound was driven by
36 increased brine rejection from sea ice formation, triggered by nearly equal effects of local
37 anomalous winds and surface heat flux. The local divergent wind anomalies promoted local
38 sea ice formation by creating a thin ice area, while cooling heat flux anomaly decreased the
39 surface temperature, increasing sea ice production as well. This highlights the importance of
40 understanding local climate variability in projecting future dense shelf water change.

41

42

43

44

45 **Plain Language Summary**

46 Previous research linked the recent salinity increase in the western Ross Sea to weakened
47 easterly winds from the Amundsen Sea. However, insufficient observations limit the further
48 investigation of the linkage and underlying mechanisms between atmospheric forcing and
49 shelf water salinity changes. In this study, we use a global ocean-sea ice coupled model to
50 investigate the factors affecting the recent western Ross Sea shelf water salinity increase.
51 Based on a surface salinity budget analysis, we show that the recent salinity increase was
52 supplied by brine rejection induced by increased sea ice formation, triggered almost equally
53 by local anomalous winds and surface heat flux. The local wind anomalies induced a
54 divergent motion in sea ice, reducing sea ice thickness and promoting local sea ice formation.
55 Meanwhile, a negative heat flux anomaly from the atmosphere cools the surface, increasing
56 sea ice production as well. Our study highlights the impact of local climate variability on
57 dense shelf water. Moreover, the model experiment design and salinity budget analysis
58 undertaken here provide an essential reference for identifying the major drivers of the shelf
59 water salinity variations.

60
61
62
63
64
65
66
67

68 **1. Introduction**

69 The Ross Sea provides the densest Dense Shelf Water (DSW), the precursor for Antarctic
70 bottom water (AABW) on its continental shelf and contributes approximately 25% of AABW
71 formation to the global ocean (**Figure 1a**; Orsi et al., 2002). Water in the western Ross Sea
72 shelf is particularly important for AABW formation due to its high salinity, resulting from
73 local salt inputs produced during sea ice formation (Sansiviero et al., 2017), together with
74 remote sources advected toward the western Ross Sea by coastal currents (Jendersie et al.,
75 2018).

76 In the western Ross Sea, sea ice is driven northward by the persistent, strong southerly winds.
77 During the austral winter (April-October), this results in vigorous sea ice formation and brine
78 release, which initiates the formation of high-salinity shelf water and determines its
79 properties (Rusciano et al., 2013; Morrison et al., 2023). Moreover, the ocean circulation on
80 the Ross Sea continental shelf consists of two main inflows from the east driven by the
81 easterly wind, the Antarctic Coastal Current and Antarctic Slope Current (Smith Jr et al.,
82 2012). Thus, these westward inflows are essential in transporting fresher water from the
83 upstream Amundsen Sea to the Ross Sea (**Figure 1a**), influencing the long-term variability of
84 DSW salinity in the western Ross Sea (Jacobs et al., 2022).

85 Ocean measurements in the western Ross Sea have shown a significant decrease (~ 0.03
86 psu/dec) in DSW salinity from 1958 to 2008 (Jacobs & Giulivi, 2010), which is thought to be
87 driven by enhanced Antarctic melting in the Amundsen Sea (Nakayama et al., 2014). During
88 2012-2018, however, the DSW salinity in the western Ross Sea experienced a sharp rebound,
89 with values in 2018 comparable to those in the mid-late 1990s (Castagno et al., 2019). This
90 salinity rebound contradicts the ongoing increased Antarctic meltwater, which would
91 continue to decrease rather than increase DSW salinity in the western Ross Sea (Jacobs et al.,
92 2022). Silvano et al. (2020), based on in-situ observations, linked this salinity recovery to the

93 enhanced sea ice formation driven by weakened easterly winds from the Amundsen Sea.
94 Jacobs et al. (2022) discussed the short-term variability related to the Interdecadal Pacific
95 Oscillation, zonal winds, and ice shelf melting in the Amundsen Sea. However, insufficient
96 observations limit a more comprehensive analysis of the individual physical interactions
97 among the atmosphere, ocean, and sea ice that influence recent salinity variations in the
98 western Ross Sea. In this work, we used a well-tuned global ocean sea-ice model and
99 perturbation experiments to isolate the response of shelf water salinity in Terra Nova Bay
100 (TNB, 74.25–75.50° S, 163–166° E; **Figure 1a**) to various surface forcing, aiming to unravel
101 the cause of the observed salinity rebound. Our study highlights the importance of integrating
102 observational data with model studies.

103 **2. Model and experiment design**

104 *2.1 In situ hydrographic data*

105 This study used in-situ salinity observations from Castagno et al. (2019) for 1995-2018, that
106 were primarily obtained during summer. Hydrographic measurements in TNB and other
107 nearby regions (Supplementary Text 1.1 and **Figure S1**) with station depths deeper than
108 800m have been used. These regions chosen are representative of DSW conditions in the
109 western Ross Sea with a marked rebound in salinity during 2012-2018 (**Figures 1b, S1**). To
110 compare with observations, model results are sampled in the same area for those years in
111 which the observation data were taken.

112 *2.2 Model description*

113 We adopted the Australian Community Climate and Earth System Simulator – Ocean Model
114 2 (ACCESS-OM2) (Kiss et al., 2020) with a configuration of 1° horizontal resolution. The
115 atmospheric forcing was derived from JRA55-do (Tsujino et al., 2018). While this model
116 does not include the ice shelf component, the Antarctic calving and ice shelf basal melting are

117 prescribed (Depoorter et al., 2013) as a climatological runoff at the surface. After a 200-year
 118 spin-up under repeated 1990-1991 JRA55-do forcing, the model reached quasi-equilibrium
 119 and was then forced with the 3-hourly JRA55-do interannual year forcing for 29 years from 1
 120 January 1990 to 31 December 2018. All the experiments used a non-adaptive salinity
 121 relaxation scheme which prevents model mean state from drifting too much but still allows
 122 free responses to the applied surface forcing perturbations (Zhang & McPhaden, 2008; Lyu et
 123 al., 2023). Refer to Supplementary Text 1.4 for details. Our analysis focuses on the recent
 124 period 2000–2018, using annual data from model simulations and observations for
 125 comparison.

126 *2.3 Surface salinity budget analysis*

127 At the surface, the ocean salinity budget in a grid cell is given by:

$$\frac{\partial S}{\partial t} = -\nabla \cdot (\mathbf{u}S) + \nabla \cdot (K_{eddy}S) + \nabla \cdot (K_{small}S) + Res + \frac{(E-P-R)S}{h} + \frac{\rho_I I(S-S_I)}{\rho_o h} \quad (1)$$

128 where S is sea surface salinity, $\partial S/\partial t$ is the salinity tendency, h is the grid cell thickness, and
 129 \mathbf{u} is the three-dimension velocity. K_{eddy} is the diffusion tensor for mesoscale mixing, and
 130 K_{small} represents vertical diffusion and other mixing processes smaller than eddies. Res is the
 131 surface salinity relaxation. E and P are the rates of evaporation and precipitation respectively
 132 (positive upward), and R is river runoff and meltwater from Antarctica and Greenland. I is
 133 the rate of sea ice formation while S_I is sea ice salinity. ρ_o and ρ_I are the reference seawater
 134 density and sea ice density, respectively.

135 The salinity budget in Eq.1 states that the time tendency of salinity (left-hand side) equals all
 136 contributing terms (right-hand side), including salt convergences due to the combined oceanic
 137 processes and salinity relaxation (i.e., advection, the first term; diffusion, the second and third
 138 term; and relaxation, the fourth term), net precipitation, runoff and meltwater, and sea ice.

139 Since the focus of this research is on the recent salinity rebound, the linear trend from 2000 to

140 2018 has been removed from each term on both sides prior to the budget analysis calculation.
141 We then use these salinity budget terms to isolate the respective contributions of these
142 processes to the salinity rebound in our perturbation experiment.

143 *2.4 Experiment design*

144 We designed three perturbation experiments over 2010 to 2018 to investigate the role of
145 surface forcing in the rebound of shelf water salinity (Supplementary Table S1). In the first
146 experiment, the All-Vary experiment, the ACCESS-OM2 model is forced with prescribed
147 atmospheric conditions taken from the JRA55-do 3-hourly forcing from 2010 to 2018. In the
148 second experiment, the Wind-Vary experiment, the wind forcing is the same as in the All-
149 Vary experiment, but the rest of the atmospheric forcing is replaced by the 3-hourly
150 climatological forcing (derived over the 2000-2010 base period) in the Southern Hemisphere
151 (south of 0°). In the third experiment from, the All-Fixed experiment, all the atmospheric
152 forcing is replaced by the 2000-2010 climatological forcing in the Southern Hemisphere.
153 Applying a 3-hourly climatology out of a 10-year base period may suppress high-frequency
154 storm forcing. To test this, we have also conducted another fixed-forcing experiment using
155 2009-2010 (1st May 2009 to 30th April 2010) repeat year forcing (All-Fixed 09-10), which
156 preserves high-frequency forcing and shows similar results as the All-Fixed experiment
157 (Supplementary Text 1.5 and **Figure S2**).

158 In ACCESS-OM2, the ocean and sea ice models are forced by the surface heat flux,
159 freshwater flux, and wind stress calculated on-the-fly from prescribed atmospheric conditions
160 and model states. The ongoing increased Antarctic meltwater (Adusumilli et al., 2020) can
161 not explain the observed rapid salinity rebound (Jacobs et al., 2022; Yan et al., 2023). Other
162 freshwater flux, including precipitation, evaporation, and runoff, has a minimal impact on the
163 salinity in the western Ross Sea (Porter et al., 2019). Therefore, changes in surface forcing in
164 the study region are mainly from surface heat flux and wind stress. We then compared the

165 Wind-Vary experiment versus the All-Fixed experiment to isolate the impact of wind stress ,
166 and similarly compared the All-Vary experiment versus the Wind-Vary experiment to isolate
167 the shelf water salinity response to surface heat flux anomaly. Note that wind anomalies can
168 lead to anomalies in turbulent heat flux. However, we have checked the difference between
169 Wind-Vary and All-Fixed experiments and found that the wind-induced heat flux anomalies
170 are relatively small compared to the heat flux anomalies between All-Vary and Wind-Vary
171 experiments (**Figure S3**). Furthermore, we found that decomposition of total salinity changes
172 into wind-driven and heat flux-driven components achieves a good closure, i.e., the sum of
173 the two components is nearly equal to the total signal.

174 **3. Results**

175 *3.1 Observed salinity variations in the western Ross Sea reproduced by model simulation*

176 **Figure 1** shows the map of the study area, and the observed and modelled salinities over
177 different depth ranges in the western Ross Sea. The decreasing trend of DSW salinity near the
178 seafloor before 2010 is estimated to be -0.05 psu/dec (**Figure 1b**, red line), slightly larger
179 than the long-term trend of -0.03 - 0.04 psu/dec estimated by Jacobs et al. (2002) and Jacobs
180 and Giulivi (2010). However, after reaching a minimum in around 2012, the freshening trend
181 appears to reverse with a rapid salinity rebound (**Figure 1b**, red line). The DSW salinity in
182 TNB had rebounded up to 2018, indicating a recent recovery of DSW salinity in the western
183 Ross Sea (Castagno et al., 2019). The observed decrease of DSW salinities between 2000 and
184 2010 followed by the sharp rebound is reproduced well by our model simulation based on
185 ACCESS-OM2 (**Figure 1b**, red and black lines, $r=0.73$, $p<0.05$).

186 This recent sharp salinity rebound is simulated throughout the entire water column from
187 surface to the bottom (**Figures 1b,c,d,S1**), supported by a strong correlation, with surface

188 salinity leading seafloor salinity at a maximum of 16 months ($r=0.69$, $p<0.05$). We then
189 discuss the drivers of the recent DSW salinity rebound based on our model simulation.

190 *3.2 The effects of surface forcing on recent salinity rebound through sea ice formation*

191 A surface salinity budget analysis based on our model simulation (**Figure 2a**) reveals that
192 increased brine rejection from sea ice production largely drives the recent salinity rebound
193 over the western Ross Sea between 2010 and 2018. Oceanic processes and salinity relaxation
194 counteract the salinity tendency implied by sea ice brine rejection. Other freshwater sources,
195 such as net precipitation and runoff, exert minimal impact and cannot explain the observed
196 rapid DSW salinity rebound. This is substantiated by hydrographic measurements that neither
197 support a reduced net precipitation over the Ross Sea continental shelf (Porter et al., 2019)
198 nor evidence of a decline in freshwater inflow from the Amundsen Sea (Adusumilli et al.,
199 2020).

200 To further determine which surface forcing is responsible for the recent salinity rebound, we
201 conduct three perturbation experiments: All-Fixed, Wind-Vary, and All-Vary. In the All-
202 Fixed experiment, with atmospheric forcing remaining fixed to its climatology from 2000 to
203 2010, a negative trend in the salinity of the DSW is simulated (-0.062 psu/dec 2011-2018, red
204 line in **Figure 2b**), which is roughly consistent with the declining trend observed from the
205 1990s to the early 2010s. The All-Fixed experiment suggests that a continued decrease in
206 DSW salinity would be expected in the absence of changes in atmospheric conditions. The
207 Wind-Vary experiment suggests that incorporating real-time wind forcing could basically
208 stop the gradual decrease trend in salinity observed previously over 2000-2010 and stabilize
209 without any obvious trends over 2010-2018 (**Figure 2b**, blue line). It is important to note that
210 besides wind stress, surface heat flux also plays a significant role in sea ice formation. Sea ice
211 formation is closely connected to surface air temperature and sea surface temperature, which,
212 in turn, is influenced by various types of surface heat flux from the atmosphere. Our model

213 experiments thus indicate that the dynamic process (sea ice formation driven by wind stress
214 anomaly) and thermodynamic process (sea ice formation driven by surface heat flux
215 anomaly) have comparable impacts on the recent rebound in DSW salinity, contributing ~
216 0.050 psu/dec each to the rebound (**Figure 2b**).

217 We next show the processes and mechanisms that explain how wind forcing (comparing
218 Wind-Vary and All-Fixed experiments) and surface heat flux (comparing All-Vary and
219 Wind-Vary experiments) cause increased sea ice production that further induces the recent
220 rebound of DSW salinity in the western Ross Sea.

221 *3.3 Increased sea ice formation driven by anomalous wind forcing*

222 Sea ice dynamical processes, such as a changed sea ice motion in response to changing
223 surface wind stress, play an important role in the redistribution of sea ice (Holland & Kwok,
224 2012). Ice motion is described by ice velocity, whereas sea ice advection is described here by
225 sea ice convergence $[-\nabla \cdot (\mathbf{u}h)]$ (**Figures 3c,d**), where \mathbf{u} is sea ice velocity and h is sea ice
226 thickness (Zhang et al., 2010). Thus, changes in ice thickness (mass gain or loss) due to ice
227 advection quantitatively describe the impact of wind-driven ice motion on sea ice spatial
228 redistribution.

229 Mass loss due to sea ice advection generally occurs in the south region of the western Ross
230 Sea, and ice gain occurs in the north (**Figure 3c**), indicating a sea ice motion from south to
231 north in the Western Ross Sea. Such a sea ice advection pattern is attributed to strong
232 northward ice motion driven by the coastal currents and strong southerly winds prevailing in
233 winter (Turner et al., 2016). During the period of 2014-2017, however, a local wind stress
234 anomaly in the western Ross Sea displayed a divergent pattern (**Figure 3b**, blue shading).
235 This anomaly had a notable impact on the motion of sea ice, particularly in impeding its
236 northward motion, resulting in ice loss in the western Ross Sea (**Figure 3d**, blue shading,

237 change in ocean circulation is negligible in our Wind-Vary experiment) and concurrent ice
238 gain in the Ross Sea polynya near the coast (**Figure 3d**, red shading). Consequently, local
239 changes in ice thickness (gain and loss) due to this reduced northward ice transport can be up
240 to 0.2 m, leading to the expansion of a larger area of thin ice in the north and a narrow area of
241 thick ice near the coast (**Figure S4**). This increased presence of thin ice contributes to an
242 overall increased ice production in the western Ross Sea continental shelf (0.17cm/day in
243 162-168°E, 73-78°S, **Figure 3f**), as growth rates of thin ice are higher compared to thick ice
244 (Zhang et al., 2010).

245 The significant negative spatial correlation between the simulated anomalies of sea ice
246 advection and sea ice production (**Figures 3d,f**, $r = -0.73$, $p < 0.01$) further highlights the close
247 relationship between wind-driven sea ice mass advection and ice production. Additionally,
248 the sea ice loss (gain) resulting from sea ice mass advection exhibits a significant correlation
249 with the wind divergence anomaly over the western Ross Sea (**Figures 3b,d**, $r = 0.67$,
250 $p < 0.01$). These findings suggest that, in the Wind-Vary experiment, wind forcing plays a
251 dominant role in the formation of ice in the Ross Sea, primarily through ice mass advection
252 processes. To further identify the region where the wind forcing is responsible for the
253 changes in sea ice, we conducted a specific Ross Sea-Only wind experiment (Supplementary
254 Text 1.5 and **Figure S5**). Our investigation reveals that only when applying real-time wind
255 forcing in the western Ross Sea region (160°E-170°W, 60°S-80°S) the model can successfully
256 simulate the increased salinity of DSW driven by wind (**Figures S5,S6**). This suggests that
257 the wind-driven component of the simulated increase in DSW salinity is primarily driven by
258 local wind anomalies rather than non-local wind from distant regions, distinguishing our
259 work from the previous study by Silvano et al. (2020). Thus, during the period of 2014-2017,
260 the amplified sea ice production and brine rejection observed in the Wind-Vary experiment in

261 the western Ross Sea can be attributed to the thinning of sea ice caused by local divergent
262 wind anomalies.

263 *3.4 Increased sea ice formation driven by surface heat flux*

264 In addition to the dynamical processes induced by wind, thermodynamic processes can also
265 play an important role in the production of sea ice. During the sea ice growth season, the
266 surface heat flux plays a crucial role in influencing sea ice production by affecting the sea
267 surface temperature (Holland et al., 2010). During the period of 2014-2017, a comparison
268 between All-Vary and Wind-Vary model experiments reveals that with a decrease in surface
269 heat flux from the atmosphere, there is a corresponding decrease in upper-ocean temperature
270 (**Figures 4b,d**) in the western Ross Sea. This decrease in temperature promotes an increase in
271 sea ice growth, resulting in increased brine rejection from the new ice and subsequently
272 contributing to an increased salinity from surface to seafloor in the western Ross Sea
273 (**Figures 2b,4f**). The significant spatial correlation between the anomalies of surface heat flux
274 and sea surface temperature (**Figures 4b,d**, $r = 0.68$, $p < 0.01$), and sea ice production
275 (**Figures 4b,f**, $r = 0.63$, $p < 0.01$) further highlights the strong connection between surface heat
276 flux and sea ice production.

277 It is essential to note that contrary to a simplistic inverse correlation, the relationship between
278 sea surface temperature and net sea ice production is more intricate (Zhang, 2007). Our
279 simulations indicate that in the upper 200 meters of the western Ross Sea, an increase in
280 salinity and a decrease in temperature lead to increased ocean density (**Figure S7**). This
281 increased upper-ocean density in turn reduces stratification (the denser layer above the lighter
282 layer) and enhances vertical heat exchange, leading to a greater upward ocean heat transport
283 available to melt the sea ice (Zhang, 2007). The pivotal balance of sea ice thus lies between
284 the initial sea ice growth driven by surface cooling and the sea ice melt induced by vertical
285 heat flux from the subsurface. In line with this, our model exhibits a positive anomaly in local

286 net ice production of 0.2 cm/day (163-170°E, 72-78°S, **Figure 4f**), primarily driven by a more
287 pronounced increase in ice growth compared to ice melt (**Figure S8**). Hence, the overall
288 increase in net sea ice production and brine rejection due to the thermodynamic process is
289 driven by the rate of ice growth—induced by lower surface temperatures—surpassing the rate
290 of ice melt, which itself is influenced by increased convective overturning and resultant
291 upward ocean heat transport.

292 **4. Discussion and conclusions**

293 This study presents results from a model study of the recent rebound of DSW salinity in the
294 western Ross Sea. Based on a well-tuned global ocean-sea ice model, surface salinity budget
295 analysis shows that the recent salinity rebound is dominated by increased brine rejection from
296 sea ice formation, which further propagates and extends through the whole water column
297 from surface to seafloor (0-900 m). We further conduct three main model perturbation
298 experiments and two additional ones, finding that this increased sea ice formation is driven
299 by the combined effect of anomalous local wind stress and surface heat flux, which have
300 nearly equal impacts on shelf water salinity rebound through dynamic and thermodynamic
301 processes. During 2014-2017, the local wind anomalies induced a divergent motion in sea
302 ice, reducing sea ice thickness and promoting local sea ice formation. Meanwhile, cooling
303 heat flux anomaly from the atmosphere cools the surface, increasing sea ice production in
304 winter.

305 The Southern Oscillation Index (SOI) captures climate variability associated with the ENSO
306 events, influencing the low-pressure system over the Amundsen Sea (Amundsen Sea Low,
307 ASL) through atmospheric teleconnections (Lee & Jin, 2023). A negative SOI (El Niño
308 event) over 2014-2017 (**Figure S9a**) influenced an eastward and northward shift of the ASL
309 center (**Figure S9b**) (Raphael et al., 2016), leading to a reduction in the zonal sea level
310 pressure gradient in the western Ross Sea (**Figures S9c,d**) (Coggins & McDonald, 2015),

311 thus weakening southerlies and reducing surface heat flux in the western boundary (Clem et
312 al., 2017), which likely contributed to the recent rebound of DSW salinity through sea ice
313 formation.

314 The model's 1° resolution might not be able to fully resolve ocean-sea ice interactions,
315 especially in the Ross Sea polynyas (Kurtakoti et al., 2021). While the model does simulate
316 the overall trend shift quite well, it tends to slightly underestimate the mean sea ice
317 production in the Ross Sea compared to observations (**Figure S10**). Moreover, in the absence
318 of a quantitative estimate of upstream freshwater flux, we are unable to conduct a detailed
319 budget analysis to accurately assess the contribution of Antarctic meltwater. Nonetheless,
320 recent studies suggested an acceleration in freshwater flux in the upstream Ross Sea and
321 Amundsen Sea in the past decades (Adusumilli et al., 2020; Jacobs et al., 2022), likely
322 contributing to lower, rather than higher, surface salinity in the western Ross Sea. Therefore,
323 this further indicates the significant contribution of sea ice production driven by local surface
324 forcing to the recent DSW salinity rebound.

325 Long-term observations have recorded a freshening AABW in the Ross Sea over the past 60
326 years (Jacobs et al., 2022), likely as a result of increased Antarctic meltwater (Lago &
327 England, 2019). Our study reveals that climate variability and local surface forcing can
328 temporally counteract this long-term freshening by enhancing sea ice formation. With
329 Antarctic sea ice setting several record lows in recent years (Purich & Doddridge, 2023), the
330 salinity rebound discussed here is unlikely to be sustained and has the possibility of reverting
331 to the freshening trend (Jacobs et al., 2022). However, future climate projections show an
332 increased frequency of extreme El Niño events (Cai et al., 2014). Based on the mechanism
333 demonstrated here, this is likely to influence a north-eastward shift of the ASL center, thereby
334 enhancing AABW formation that potentially offsets or even surpasses the meltwater-induced
335 freshening on different time scales. Moreover, our experiment design and salinity budget

336 analysis conducted here provide an essential reference for identifying the major drivers of the
337 shelf water salinity variations from interannual to decadal time scales.

338

339 **Acknowledgments**

340 This research was supported by the Australian Research Council Special Research Initiative,
341 the Australian Centre for Excellence in Antarctic Science (Project Number SR200100008),
342 Australian National Environmental Science Program (NESP) Climate System Hub (Project
343 CS2.10), and the Centre for Southern Hemisphere Oceans Research (CSHOR), jointly funded
344 by the Commonwealth Scientific and Industrial Research Organisation (CSIRO, Australia)
345 and the Qingdao National Laboratory for Marine Science and Technology (QNLN, China).

346 This research was undertaken with the assistance of resources from the Australian National
347 Computational Infrastructure (NCI). The authors thank the Consortium for Ocean-Sea Ice
348 Modelling in Australia (COSIMA; <http://www.cosima.org.au>) for making the ACCESS-OM2
349 suite of models available at <https://github.com/COSIMA/access-om2>.

350 **Open research**

351 The oceanographic data utilized in this study were sourced from the work of Castagno et al.
352 (2019). The Southern Oscillation Index (SOI) is available at
353 ([https://climatedataguide.ucar.edu/climate-data/southern-oscillation-indices-signal-noise-and-](https://climatedataguide.ucar.edu/climate-data/southern-oscillation-indices-signal-noise-and-tahitidarwin-slp-soi)
354 [tahitidarwin-slp-soi](https://climatedataguide.ucar.edu/climate-data/southern-oscillation-indices-signal-noise-and-tahitidarwin-slp-soi)). The monthly location of ASL central was also used in this study,
355 sourced from (https://scotthosking.com/asl_index). The time series of ice production in the
356 Ross Sea polynyas in Supporting Information were sourced from the work of Nihashi et al.
357 (2023). The model source code and configurations are available from
358 (<https://github.com/COSIMA/access-om2/>). The full model output is available in Zhang
359 (2023).

360 **Figure 1 | Recent Recovery of DSW salinity in the Western Ross Sea.** (a) Map of the Ross
361 Sea and the study area in TNB (solid box). Bottom topography (m) is shown in color
362 (Amante & Eakins, 2009). White and black dashed lines represent the general currents along
363 the shelf break and on the shelf, referred to in Smith et al. (2014). (b) Time series of averaged
364 DSW measured salinity (solid red line) and simulated salinity (solid black line) near the
365 seafloor, as well as the simulated salinity anomalies at different depth ranges from surface to
366 700 m (dashed lines) and their leading correlations with salinity near the seafloor. Simulated
367 zonal-averaged (163-170°E) salinity trends from 2000-2010 (c) and 2011-2018 (d).

368 **Figure 2 | Recent Recovery of DSW salinity induced by atmospheric forcing.** (a) Time
369 series of model simulated surface salinity anomalies (red line) in western Ross Sea (162°E-
370 168°E, 74°S-78°S), and time-integrated surface salinity changes due to sea ice (blue line), net
371 precipitation plus runoff (grey line), and the combined oceanic process and relaxation (green
372 line). Linear trends over 2000-2018 are removed to focus on the variability. (b) Time series
373 of averaged DSW salinity simulated by All-Vary (black line) from 2000 to 2018, Wind-Vary
374 (blue line) and All-Fixed (red line) and their trends (dashed lines) from 2011 to 2018 near the
375 seafloor in TNB. Trend values are given in the legend in psu per decade.

376 **Figure 3 | Increased sea ice production due to sea ice divergence induced by wind**
377 **anomalies.** Climatology and 2014-2017 anomalies of winds (a,b, vectors, with colour
378 shading represents wind divergence; negative values denote divergent), sea ice advection [
379 $\nabla \bullet \mathbf{u}h$] (c,d, sea ice motion and sea ice mass advection), and sea ice production (e,f) induced
380 by wind forcing. Left panel: All-Fixed, right panel: Wind-Vary minus All-Fixed.

381 **Figure 4 | Increased sea ice production due to lower temperatures induced by surface**
382 **heat flux anomalies.** Climatology and 2014-2017 anomalies of surface heat flux (Wm^{-2} ;
383 positive downward) (a,b), sea surface temperature ($^{\circ}\text{C}$) (c,d) and sea ice production (cm/day)

384 (e,f) induced by atmospheric forcing other than wind. Left panel: Wind-Vary, right panel:
385 All-Vary minus Wind-Vary.

386

387

388 **Reference**

389 Ackley, S., Stammerjohn, S., Maksym, T., Smith, M., Cassano, J., Guest, P., et al. (2020).

390 Sea-ice production and air/ice/ocean/biogeochemistry interactions in the Ross Sea during the
391 PIPERS 2017 autumn field campaign. *Annals of Glaciology*, 61(82), 181-195.

392 Adusumilli, S., Fricker, H. A., Medley, B., Padman, L., & Siegfried, M. R. (2020).

393 Interannual variations in meltwater input to the Southern Ocean from Antarctic ice shelves.

394 *Nature geoscience*, 13(9), 616-620.

395 Alekseev, G., Vyazilova, A., & Smirnov, A. (2022). Influence of Sea Surface Temperature in
396 the Tropics on the Antarctic Sea Ice during Global Warming. *Journal of Marine Science and*
397 *Engineering*, 10(12), 1859.

398 Amante, C., & Eakins, B. W. (2009). ETOPO1 arc-minute global relief model: procedures,
399 data sources and analysis.

400 Bamber, J., Van Den Broeke, M., Ettema, J., Lenaerts, J., & Rignot, E. (2012). Recent large
401 increases in freshwater fluxes from Greenland into the North Atlantic. *Geophysical research*
402 *letters*, 39(19).

403 Cai, W., Borlace, S., Lengaigne, M., Van Rensch, P., Collins, M., Vecchi, G., et al. (2014).

404 Increasing frequency of extreme El Niño events due to greenhouse warming. *Nature Climate*
405 *Change*, 4(2), 111-116.

406 Castagno, P., Capozzi, V., DiTullio, G. R., Falco, P., Fusco, G., Rintoul, S. R., et al. (2019).

407 Rebound of shelf water salinity in the Ross Sea. *Nature Communications*, 10(1), 1-6.

408 Clem, K. R., Renwick, J. A., & McGregor, J. (2017). Large-scale forcing of the Amundsen

409 Sea low and its influence on sea ice and West Antarctic temperature. *Journal of Climate*,

410 30(20), 8405-8424.

- 411 Coggins, J. H., & McDonald, A. J. (2015). The influence of the Amundsen Sea Low on the
412 winds in the Ross Sea and surroundings: Insights from a synoptic climatology. *Journal of*
413 *Geophysical Research: Atmospheres*, 120(6), 2167-2189.
- 414 Depoorter, M. A., Bamber, J. L., Griggs, J. A., Lenaerts, J. T., Ligtenberg, S. R., van den
415 Broeke, M. R., & Moholdt, G. (2013). Calving fluxes and basal melt rates of Antarctic ice
416 shelves. *Nature*, 502(7469), 89-92.
- 417 Griffies, S. M. (2012). Elements of the modular ocean model (MOM). GFDL Ocean Group
418 Tech. Rep, 7(620), 47.
- 419 Griffies, S. M., Biastoch, A., Böning, C., Bryan, F., Danabasoglu, G., Chassignet, E. P., et al.
420 (2009). Coordinated ocean-ice reference experiments (COREs). *Ocean Modelling*, 26(1-2), 1-
421 46.
- 422 Holland, M. M., Serreze, M. C., & Stroeve, J. (2010). The sea ice mass budget of the Arctic
423 and its future change as simulated by coupled climate models. *Climate dynamics*, 34, 185-
424 200.
- 425 Holland, P. R., & Kwok, R. (2012). Wind-driven trends in Antarctic sea-ice drift. *Nature*
426 *Geoscience*, 5(12), 872-875.
- 427 Hosking, J. S., Orr, A., Bracegirdle, T. J., & Turner, J. (2016). Future circulation changes off
428 West Antarctica: Sensitivity of the Amundsen Sea Low to projected anthropogenic forcing.
429 *Geophysical research letters*, 43(1), 367-376.
- 430 Hunke, E., Lipscomb, W., Turner, A., Jeffery, N., & Elliott, S. (2015). CICE: The Los
431 Alamos Sea ice Model Documentation and Software User's Manual Version 5 (Tech. Rep.
432 LA-CC-06-012). Los Alamos, NM: Los Alamos National Laboratory.
- 433 Jacobs, & Giulivi. (2010). Large multidecadal salinity trends near the Pacific–Antarctic
434 continental margin. *Journal of climate*, 23(17), 4508-4524.
- 435 Jacobs, Giulivi, & Mele, P. (2002). Freshening of the Ross Sea during the late 20th century.
436 *Science*, 297(5580), 386-389.
- 437 Jacobs, Giulivi, C., & Dutrieux, P. (2022). Persistent Ross Sea freshening from imbalance
438 West Antarctic ice shelf melting. *Journal of Geophysical Research: Oceans*, 127(3),
439 e2021JC017808.

- 440 Jendersie, S., Williams, M. J., Langhorne, P. J., & Robertson, R. (2018). The density-driven
441 winter intensification of the Ross Sea circulation. *Journal of Geophysical Research: Oceans*,
442 123(11), 7702-7724.
- 443 Kiss, A. E., Hogg, A. M., Hannah, N., Boeira Dias, F., Brassington, G. B., Chamberlain, M.
444 A., et al. (2020). ACCESS-OM2 v1. 0: a global ocean–sea ice model at three resolutions.
445 *Geoscientific Model Development*, 13(2), 401-442.
- 446 Kurtakoti, P., Veneziani, M., Stössel, A., Weijer, W., & Maltrud, M. (2021). On the
447 generation of Weddell Sea polynyas in a high-resolution Earth system model. *Journal of*
448 *Climate*, 34(7), 2491-2510.
- 449 Lago, V., & England, M. H. (2019). Projected slowdown of Antarctic bottom water formation
450 in response to amplified meltwater contributions. *Journal of climate*, 32(19), 6319-6335.
- 451 Lee, H.-J., & Jin, E. K. (2023). Understanding the delayed Amundsen Sea low response to
452 ENSO. *Frontiers in Earth Science*, 11, 1136025.
- 453 Lyu, K., Zhang, X., Church, J. A., Wu, Q., Fiedler, R., & Dias, F. B. (2023). Roles of Surface
454 Forcing in the Southern Ocean Temperature and Salinity Changes under Increasing CO₂:
455 Perspectives from Model Perturbation Experiments and a Theoretical Framework. *Journal of*
456 *Physical Oceanography*, 53(1), 19-36.
- 457 Morrison, A. K., Huneke, W. G., Neme, J., Spence, P., Hogg, A. M., England, M. H., &
458 Griffies, S. M. (2023). Sensitivity of Antarctic shelf waters and abyssal overturning to local
459 winds. *Journal of climate*, 1-32.
- 460 Nakayama, Y., Timmermann, R., Rodehacke, C. B., Schröder, M., & Hellmer, H. H. (2014).
461 Modeling the spreading of glacial meltwater from the Amundsen and Bellingshausen Seas.
462 *Geophysical research letters*, 41(22), 7942-7949.
- 463 Nihashi, S., & Ohshima, K. I. (2015). Circumpolar mapping of Antarctic coastal polynyas
464 and landfast sea ice: Relationship and variability. *Journal of Climate*, 28(9), 3650-3670.
- 465 Nihashi, S., Ohshima, K. I., & Tamura, T. (2017). Sea-ice production in Antarctic coastal
466 polynyas estimated from AMSR2 data and its validation using AMSR-E and SSM/I-SSMIS
467 data. *IEEE Journal of Selected Topics in Applied Earth Observations and Remote Sensing*,
468 10(9), 3912-3922.

- 469 Nihashi, S., Ohshima, K. I., & Tamura, T. (2023). Reconstruct the AMSR-E/2 thin ice
470 thickness algorithm to create a long-term time series of sea-ice production in Antarctic
471 coastal polynyas. *Polar Science*, 100978.
- 472 Orsi, A. H., Smethie Jr, W. M., & Bullister, J. L. (2002). On the total input of Antarctic
473 waters to the deep ocean: A preliminary estimate from chlorofluorocarbon measurements.
474 *Journal of Geophysical Research: Oceans*, 107(C8), 31-31-31-14.
- 475 Porter, D. F., Springer, S. R., Padman, L., Fricker, H. A., Tinto, K. J., Riser, S. C., et al.
476 (2019). Evolution of the seasonal surface mixed layer of the Ross Sea, Antarctica, observed
477 with autonomous profiling floats. *Journal of Geophysical Research: Oceans*, 124(7), 4934-
478 4953.
- 479 Purich, A., & Doddridge, E. W. (2023). Record low Antarctic sea ice coverage indicates a
480 new sea ice state. *Communications Earth & Environment*, 4(1), 314.
- 481 Raphael, M. N., Marshall, G., Turner, J., Fogt, R., Schneider, D., Dixon, D., et al. (2016).
482 The Amundsen Sea low: Variability, change, and impact on Antarctic climate. *Bulletin of the*
483 *American Meteorological Society*, 97(1), 111-121.
- 484 Rusciano, E., Budillon, G., Fusco, G., & Spezie, G. (2013). Evidence of atmosphere–sea ice–
485 ocean coupling in the Terra Nova Bay polynya (Ross Sea—Antarctica). *Continental Shelf*
486 *Research*, 61, 112-124.
- 487 Sansiviero, M., Maqueda, M. M., Fusco, G., Aulicino, G., Flocco, D., & Budillon, G. (2017).
488 Modelling sea ice formation in the Terra Nova Bay polynya. *Journal of Marine Systems*, 166,
489 4-25.
- 490 Silvano, A., Foppert, A., Rintoul, S. R., Holland, P. R., Tamura, T., Kimura, N., et al. (2020).
491 Recent recovery of Antarctic Bottom Water formation in the Ross Sea driven by climate
492 anomalies. *Nature Geoscience*, 13(12), 780-786.
- 493 Smith Jr, W. O., Sedwick, P. N., Arrigo, K. R., Ainley, D. G., & Orsi, A. H. (2012). The Ross
494 Sea in a sea of change. *Oceanography*, 25(3), 90-103.
- 495 Smith, W. O., Dinniman, M. S., Hofmann, E. E., & Klinck, J. M. (2014). The effects of
496 changing winds and temperatures on the oceanography of the Ross Sea in the 21st century.
497 *Geophysical research letters*, 41(5), 1624-1631.
- 498 Tamura, T., Ohshima, K. I., & Nihashi, S. (2008). Mapping of sea ice production for
499 Antarctic coastal polynyas. *Geophysical Research Letters*, 35(7).

- 500 Tsujino, H., Urakawa, S., Nakano, H., Small, R. J., Kim, W. M., Yeager, S. G., et al. (2018).
501 JRA-55 based surface dataset for driving ocean–sea-ice models (JRA55-do). *Ocean*
502 *Modelling*, 130, 79-139.
- 503 Turner, J., Hosking, J. S., Marshall, G. J., Phillips, T., & Bracegirdle, T. J. (2016). Antarctic
504 sea ice increase consistent with intrinsic variability of the Amundsen Sea Low. *Climate*
505 *dynamics*, 46, 2391-2402.
- 506 Valcke, S. (2006). OASIS User guide, prism 2-5, PRISM-Support Initiative. Retrieved from
- 507 Yan, L., Wang, Z., Liu, C., Wu, Y., Qin, Q., Sun, C., et al. (2023). The salinity budget of the
508 Ross Sea continental shelf, Antarctica. *Journal of Geophysical Research: Oceans*, 128(3),
509 e2022JC018979.
- 510 Zhang, J. (2007). Increasing Antarctic sea ice under warming atmospheric and oceanic
511 conditions. *Journal of climate*, 20(11), 2515-2529.
- 512 Zhang, J. (2023). A model-based investigation of the recent rebound of shelf water salinity in
513 the Ross Sea. [Dataset]. Zenodo. <https://doi.org/10.5281/zenodo.8415955>
- 514 Zhang, J., Woodgate, R., & Moritz, R. (2010). Sea ice response to atmospheric and oceanic
515 forcing in the Bering Sea. *Journal of Physical Oceanography*, 40(8), 1729-1747.
- 516 Zhang, X., & McPhaden, M. J. (2008). Eastern equatorial Pacific forcing of ENSO sea
517 surface temperature anomalies. *Journal of climate*, 21(22), 6070-6079.
- 518 Zika, J. D., Skliris, N., Blaker, A. T., Marsh, R., Nurser, A. G., & Josey, S. A. (2018).
519 Improved estimates of water cycle change from ocean salinity: The key role of ocean
520 warming. *Environmental Research Letters*, 13(7), 074036.